Accepted Manuscript: Kevin Tse, Jie Wang, Xiang Yun (2021) Structural behaviour and continuous strength method design of high strength steel non-slender welded I-section beam-columns. Thin-walled Structures. Accepted on 09/08/2021

Structural behaviour and continuous strength method design of high strength steel non-slender welded I-section beam-columns

Kevin Tse[a], Jie Wang[a,*], Xiang Yun[b,*]

[a] Department of Architecture and Civil Engineering, University of Bath, U.K.
[b] Department of Civil and Environmental Engineering, Imperial College London, London, UK

[*]Corresponding authors.
E-mail addresses: j.wang@bath.ac.uk (J. Wang); x.yun14@imperial.ac.uk (X. Yun).

Abstract

This paper presents the development of efficient design equations for high strength steel (HSS) welded I-section beam-columns under the framework of the Continuous Strength Method (CSM). The present work includes a collection of available experimental data on HSS S690 and S960 welded I-section beam-columns and a comprehensive numerical modelling programme considering a wider spectrum of parameters that influence the structural behaviour of the HSS welded I-section beam-columns. The developed FE models were first validated against test results collected from the literature, after which parametric studies were performed to generate further results to assess the accuracy of the codified design methods as used in Europe and the US, as well as to underpin new design proposals for HSS non-slender welded I-section beam-columns. It has been shown that the proposed CSM-based design approach is able to provide reliable design predictions with improved accuracy and reduced scatter over the existing design methods, and its reliability has been confirmed by means of statistical analyses.

Keywords: Beam-columns; Continuous Strength Method; Design rules; High strength steel; Finite element analysis; Reliability analysis; Welded I-sections.

1. Introduction

The Continuous Strength Method (CSM) is a deformation-based design approach that enables a more accurate allowance to be made for the spread of plasticity and allows strain hardening to be considered in a rational manner [1]. The CSM links the resistance of a cross-section to its deformation capacity through the adoption of a base curve and a material model that accurately represents the stress-strain relationship and allows for the beneficial influence of strain hardening [1]. Over the past decades, the scope of the CSM has been broadly expanded to stainless steel structures [2-7] aluminium structures [8-10], and more recently, carbon steel structures [11-18]. The CSM has gone through a systematic process of development including proposals of accurate CSM material models [2,9,12,19] and calibrations of CSM base curves [2,9,12,18], and has covered the design of cross-sections under compression [2,3,9,10,12,18], bending [2,3,5,8,9,11,12,17] and combined loading conditions [6,12-15]. Recent work on stainless steel beam-column members [6,7] has demonstrated the suitability of the application of the CSM-based design approach at the member level, particularly for cases where bending effects are dominant. It has also been argued that the beam-column member design can be further improved by using more accurate compression end points for cases where compression effects predominate [6,7]. As part of the development of the CSM framework to high strength steel (HSS) structures, this paper presents investigations of the CSM-based method for the prediction of resistances of HSS welded I-section beam-columns.

Previous studies on HSS structures have been focused mainly on the local [20-23] and global stability [24-30] of members under axial compression, where it has been found that the HSS structural members generally possess similar or higher normalised resistances than their normal strength steel counterparts, and the current design rules for HSS columns are generally conservative [24-30]. Research into the design of HSS beam-columns, especially those made of welded I-sections, remains, however, relatively scarce. The only experimental investigations on HSS welded I-section beam-columns can be found in Yang et al. [31] and Ma et al. [32,33], where specimens with steel grade S460 and S690 were tested, respectively. In these studies [31-33], improved design methods have also been proposed by simply modifying the interaction factors employed in the existing design equations, but without systematically improving the accuracy of resistance predictions for members under pure compression and pure bending, which act as the end points of the design interaction curve. The proposed interaction factors still included a large degree of compensation for the inaccurate predictions of the end points based on the existing design methods. The present paper thus aims at developing a more rational and accurate CSM-based design approach for HSS welded I-section beam-columns through a comprehensive numerical study including HSS grades of both S690 and S960.

In this paper, details of the experimental investigations carried out by Ban et al. [27] and Ma et al. [32] for HSS welded I-section columns and beam-columns are firstly summarised, followed by a comprehensive numerical investigation including validation of the developed finite element (FE) models and, based upon which, a comprehensive parametric study analysis to generate additional data considering various cross-sectional geometries, member slendernesses and loading combinations. Both the collected test results and the numerical results derived in this study were used to evaluate the existing design rules set out in Eurocode 3 [34,35] and American Specification AISC 360-16 [36] for HSS welded I-section beam-columns. Furthermore, an improved design method was also sought by adopting more accurate predictions of the end points (i.e. using revised column buckling curves for determining the column buckling strengths and the CSM [11,12] for calculating the cross-sectional bending resistances) and subsequently developed interaction factors based on these accurate end points. The proposed CSM based method is shown to give resistance predictions with enhanced accuracy and improved consistency. Finally, a reliability assessment was carried out to assess the reliability level of different design methods.

2. Summary of previous experimental investigation

The experimental investigations carried out by Ma et al. [32] for S690 welded I-section beam-columns and Ban et al. [27] for S960 welded I-section columns are summarised in this section. These data were used for the validation of the FE models as described in the following section. The material properties and the measured geometric dimensions of the test specimens are summarised in Tables 1 and 2, respectively. In Table 1, t is the thickness of the tensile coupon, E is the Young's Modulus, f_y is the yield strength, f_u is the ultimate strength and ε_u is the strain at the ultimate strength. Typical measured engineering stress-strain curves for different tensile coupon thicknesses and steel grades are illustrated in Fig. 1. In Table 2, H and B are the height and the width of the welded I-section, t_f and t_w are the flange and web thicknesses, respectively, as illustrated in Fig. 2, L is the measured length of the test specimen, L_{eff} is the effective length of the test specimen equal to the distance between the top and bottom knife-edges, v is the measured initial global geometric imperfection and e is the applied loading eccentricity which was calculated based on the strain gauge readings at the initial loading stage [32].

Figs 3 and 4 show the test setup in Ma et al. [32] and Ban et al. [27], respectively. The specimens were compressed between two parallel knife edges at the top and bottom ends, allowing the specimen ends to rotate about the minor axis. The load was applied at different eccentricities to generate a range of minor axis bending moment-to-axial load ratios. Typical failure modes of the test specimens are shown in Figs 3 and 4, revealing that failure was generally dominated by global buckling. The axial load-mid-height lateral deflection curves of typical S690 and S960 test specimens are also provided in Figs 5 and 6, respectively. The ultimate loads of all the test specimens are summarised in Table 3.

3. Numerical modelling

In this section, numerical analyses were carried out for HSS welded I-section beam-columns using the program ABAQUS of version 6.14 [37]. The developed FE models were initially validated against the collected test results on the HSS welded I-section columns and beam-columns, as summarised in Section 2, and were subsequently used to perform an extensive parametric study to generate additional numerical results covering a wider range of cross-section geometries, member slendernesses and loading combinations. The collected test results together with the numerical results were used to appraise the current design methods as well as to underpin the development of the newly proposed design method.

3.1 Description of FE models

Careful finite element (FE) modelling was first performed to replicate the HSS welded I-section column and beam-column tests [27,32]. The I-section columns and beam-columns were modelled using the four-noded shell element with reduced integration (S4R), as employed in previous similar numerical studies [6,7,14,27]. The measured geometries of the test specimens, as summarised in Table 2, were incorporated into the FE models.

To define the material properties of specimens using shell element in the ABAQUS programme, the measured engineering stress-strain curve, as illustrated in Fig. 1, must be converted into the true plastic stress-strain relationship for input into the FE shell models. The equations used for determining the true stresses σ_{true} and true plastic strains $\varepsilon_{\text{true}}^{\text{pl}}$ based on the measured engineering stress σ_{eng} and engineering strain ε_{eng} values are given by Eqs (1) and (2), respectively.

$$\sigma_{true} = \sigma_{eng}\left(1+\varepsilon_{eng}\right) \tag{1}$$

$$\varepsilon_{true}^{pl} = \ln\left(1+\varepsilon_{eng}\right) - \frac{\sigma_{true}}{E} \tag{2}$$

For the validation purpose, the weld fillets at each web-flange junction of the welled I-sections were modelled using five additional shell elements with varying thicknesses, which are determined such that the total cross-sectional area of the modelled I-section equal to that of the corresponding test specimen, as illustrated in Fig. 7. The material properties of these elements were assumed to be the same as those of the web. This approach has also been successfully employed in previous studies [11,13]. It should be noted that the weld fillets are not considered in the parametric studies.

The global geometric imperfections were considered in the FE models by taking the shape of a half-sine wave along the length of the specimen with the imperfection amplitude taken as the corresponding measured value δ, as given in Table 2. Local geometric imperfections are deemed insignificant as global instability is the focus of the present study and only non-slender cross-sections (i.e. Class 1-3 sections), where premature local buckling is unlikely to occur prior to global buckling failure, are investigated herein; thus, the local geometric imperfections were not incorporated in the FE models.

The heat input during welding would affect the material properties of the web and flanges at the adjacent regions of the web-flange junctions, yet this effect was not explicitly accounted for in the developed FE models. The welding-induced residual stresses may have a greater adverse effect on the stability of the welded I-section members, which were carefully considered by incorporating relevant residual stresses into the developed FE models. Simplified residual stress patterns, developed based on the experimental residual stress measurements [27,32], are proposed and illustrated in Figs 8(a) and (b) for S690 and S960 welded I-sections, respectively. The amplitudes recommended in the proposed residual stress models are also based on the experimental measurements [27,32] while the remaining input parameters are calculated based on stress equilibrium. It is worth noting that the flanges of the investigated S960 specimens are flame cut, resulting in tension residual stresses at the tips of the flanges (see Fig. 8(b)).

The eccentric loading was applied through two reference points which were respectively located at the centre of the top and bottom knife-edge, offsetting from the centroid of the corresponding end-section by the thickness of the knife-edge in the longitudinal direction and by a distance of the measured initial loading eccentricity e in the direction perpendicular to the bending axis. The reference points were coupled to the nodes at the corresponding end cross-section through kinematic coupling. For the boundary conditions, only the longitudinal displacement at the loading point and the minor axis rotation at both ends were unrestrained, which matched the test boundary conditions. Note that the reference points employed in the parametric studies were placed within the plane of the corresponding end section, with no offset in the longitudinal direction.

The cross-sectional mesh size was taken as the minimum value of the widths employed in the proposed residual stress patterns (i.e. a_1 -d_1 or a_2-d_2) and the plate thicknesses (i.e. t_f and t_w) to facilitate the employment of the proposed residual stress pattern while maintaining a fine mesh.

The number of elements used along the length of the specimens was taken as either 150 or $L/30$ (L in mm), depending on which is greater, to ensure that the global instability effect can be well captured.

3.2 Validation

The developed FE models were validated by comparing the experimental failure modes, the load-mid-height lateral displacement curves and the ultimate loads with those obtained from the FE models. The comparisons are shown in Figs 3-6 and Table 3. Figs 3 and 4 demonstrate that the FE models are able to capture the global failure mode accurately using the selected mesh size as described in Section 3.1. Figs 5 and 6 show that the FE models can also accurately capture the test load-mid-height lateral displacement histories. The ultimate loads from the experiments ($N_{u,test}$) and FE models ($N_{u,FEA}$) are compared in Table 3. The average values of the ratios of $N_{u,test}/N_{u,FEA}$ are 1.04 and 1.06 for the S690 and S960 specimens, respectively, indicating that the FE models can provide accurate yet slightly conservative resistance predictions of HSS welded I-section columns and beam-columns. Overall, the FE failure loads, load-mid-height lateral displacement curves, and failure modes show a good agreement with those observed in their corresponding tests, confirming the suitability of adopting the developed FE models for use in the subsequent parametric analysis.

3.3 Parametric study

Following the validation of the FE models, an extensive parametric study on HSS welded I-section beam-columns was performed considering a wider range of geometries (i.e. different cross-section slendernesses and global slendernesses), eccentricities (i.e. resulting in specimens under different compression-to-bending moment ratios) and loading conditions (i.e. compression plus major axis bending as well as compression plus minor axis bending). The obtained FE results, in combination with the available test data as summarised in Section 2, are used to evaluate the accuracy of the codified design rules set out in European (Eurocode 3: Part 1-12 [35]) and American (AISC 360-16 [36]) design standards for HSS welded I-section beam-columns, as well as a newly proposed design approach based on the Continuous Strength Method (CSM).

The geometric parameters considered in the parametric study included three cross-sectional height-to-width ratios (i.e. H/B = 1, 1.5, 2), where a constant value of B = 150 mm was adopted in all modelled specimens, three cross-section classes (under pure compression) according to the cross-section classification in EN 1993-1-12 [35] (i.e. Classes 1, 2 and 3) and six global slendernesses $\bar{\lambda}$ (i.e. $\bar{\lambda}$ = 0.3, 0.7, 1.0, 1.5, 2.0 and 2.5). It should be noted that only Classes 1, 2 and 3 cross-sections were considered in the current study as the continuous strength method has very limited benefits for the design of Class 4 cross-sections, where local buckling prevents the cross-sections from reaching significant strain hardening response. The measured stress-strain curves of the S690 (6 mm) [32] and S960 (14 mm) [27] steels were adopted in the parametric studies. The employed material stress-strain curves are shown in Fig. 1 and their key measured material properties, including the Young's modulus E, the yield strength f_y, the ultimate strength f_u and ultimate strain ε_u, are given in Table 1. The details of key parameters selected for the parametric studies are summarised in Table 4, where $\bar{\lambda}_{p,w}$ and $\bar{\lambda}_{p,f}$ are the plate slendernesses of the web and flange in pure compression, respectively. The web $\bar{\lambda}_{p,w}$ and flange $\bar{\lambda}_{p,f}$ plate slendernesses were calculated using Eqs (3)-(5) in accordance with EN 1993-1-5 [38], where $\sigma_{cr,w}$ and $\sigma_{cr,f}$ are the local buckling stresses of the web and the flange plates, respectively, k_σ is the buckling coefficient taking account of the boundary conditions and stress distribution of the plate [38], which is taken as 4 for the web plate in compression and 0.43 for the flange plate in compression, v is the Poisson's ratio taken as 0.3, and b and t

are plate width and thickness, respectively. The flange and web thicknesses were selected to get similar plate slendernesses of $\bar{\lambda}_{\mathrm{p,w}}$ and $\bar{\lambda}_{\mathrm{p,f}}$ in compression, thus minimising any significant effect of web-to-flange interaction on the ultimate resistance of welded I-section beam-columns. As in-plane bucking is the focus of the present study, lateral restraints were applied at the web-to-flange junctions to preclude lateral torsional buckling, if any, for specimens subjected to compression plus major axis bending. For all the modelled specimens, initial global imperfections were incorporated by adopting the shape of a half-sine wave along the member length with its amplitude taken as $L_{\mathrm{eff}}/1000$. This value was chosen to maintain consistency with the value assumed in the development of the EC3 column buckling curves [39] and to obtain slightly conservative results relative to those derived from FE models with a smaller imperfection amplitude of $L_{\mathrm{eff}}/1500$ as adopted in the formulation of the AISC buckling curves [36]. As discussed earlier, local geometric imperfections were not included in the FE models owing to their negligible effects on the overall stability of beam-column members made of non-slender cross-sections [7,27,33], which is the focus of the present study.

$$\bar{\lambda}_{\mathrm{p,w}} = \sqrt{\frac{f_{\mathrm{y}}}{\sigma_{\mathrm{cr,w}}}} \tag{3}$$

$$\bar{\lambda}_{\mathrm{p,f}} = \sqrt{\frac{f_{\mathrm{y}}}{\sigma_{\mathrm{cr,f}}}} \tag{4}$$

$$\sigma_{\mathrm{cr}} = k_{\sigma} \frac{\pi^2 E}{12\left(1-\nu^2\right)} \left(\frac{t}{b}\right)^2 \tag{5}$$

The load eccentricities were designed to generate a wider spectrum of load-to-bending moment ratios. A dimensionless parameter θ, reflecting the load-to-bending moment ratio, is introduced herein, as defined by Eq. (6) and illustrated in Fig. 9. In Eq. (6), N_{Ed} and M_{Ed} are the design compression load and bending moment, respectively, and N_{Rd} and M_{Rd} are design resistances for column buckling and cross-sections in bending, respectively. Note that $\theta = 0°$ represents that the specimen is under pure bending while $\theta = 90°$ indicates that the specimen is under pure compression. Eight load eccentricities were considered in the parametric study for each combination of cross-section aspect ratio, cross-section slenderness, global slenderness, buckling axis and steel grade, resulting in a total of 1728 FE models generated.

$$\theta = \tan^{-1}\left(\frac{N_{\mathrm{Ed}} / N_{\mathrm{Rd}}}{M_{\mathrm{Ed}} / M_{\mathrm{Rd}}}\right) \tag{6}$$

4. Assessment of design methods

In this section, the beam-column design rules set out in EN 1993-1-12 [35] and AISC 360-16 [36] were examined using the collected test results [27,32] and the numerical data generated in the present study. A new design approach, based on the revised column buckling curves and the Continuous Strength Method (CSM) for determining the end points of the interaction diagram as well as modified interaction factors to describe the load-moment interaction curve, was also proposed, underpinned by the experimental and numerical data. The experimental and numerical ultimate loads were compared with different design predictions, as given in Tables 5 and 6 for HSS welded I-section beam-columns under compression plus minor axis bending and compression plus major axis bending, respectively. In Tables 5 and 6, N_{u} is the experimental or numerical ultimate load, and N_{EC3}, N_{AISC} and N_{CSM} are the ultimate load predictions (N_{pred}) according to EN 1993-1-12 [35], AISC 360-16 [36], and the new proposed

CSM-based design approach, respectively. A value of N_u/N_{pred} greater than unity indicates a safe-sided prediction and vice versa. In the assessment, all calculations are based on the measured (or modelled) geometries and material properties, with all safety factors set to unity. Detailed descriptions of the Eurocode and American design rules, as well as the development of the CSM-based design approach, are given in the following sub-sections.

4.1 EN 1993-1-12 (2007) (EC3)

The current EN 1993-1-12 [35] guidance for the design of HSS welded I-section beam-columns follows generally the same approach as that for the normal strength steel set out in EN 1993-1-1 [34], the scope of which is limited to steel grades up to S700. The EC3 design formula for HSS welded I-section beam-columns is given by Eq. (7), where N_{Ed} and M_{Ed} are the design compression load and bending moment, respectively, $N_{b,Rd}$ is the column buckling resistance, $M_{EC3,Rd}$ is the cross-sectional bending resistance, and k_{EC3} is the interaction factor. The column buckling resistance ($N_{b,Rd}$) and the cross-sectional bending resistance ($M_{EC3,Rd}$) are determined according to the corresponding design rules set out in EN 1993-1-1 [34] and EN 1993-1-12 [35]. Specifically, $M_{EC3,Rd}$ is equal to the plastic bending moment M_{pl} for members with Class 1 or 2 cross-sections and equal to elastic bending moment M_{el} for members with Class 3 cross-sections. As sufficient lateral restraints were provided for specimens subjected to compression plus major axis bending, only in-plane flexural buckling shall be considered in determining the column buckling strength $N_{b,Rd}$. In the calculation of $N_{b,Rd}$ for HSS columns with welded I-sections, the buckling curves ‘a’ and ‘b’ are adopted for members in major axis buckling and minor axis buckling, respectively, as recommended in [26,27,29]. It should be noted that these buckling curves were higher than the designated ones set out in EN 1993-1-12 [35], reflecting the reducing relative influence of residual stresses on the strength reduction of column members with increasing steel grades.

$$\frac{N_{\mathrm{Ed}}}{N_{\mathrm{b,Rd}}}+k_{\mathrm{EC3}}\frac{M_{\mathrm{Ed}}}{M_{\mathrm{EC3,Rd}}}\leq 1 \tag{7}$$

Two different methods are provided in Annex A and B of EN 1993-1-1 [34] to calculate the interaction factor k_{EC3}. The Method A addresses the individual structural effects on the interaction factor while its calculation procedures are too complicated for practical use; the Method B provides simpler equations for the determination of the interaction factor k_{EC3} considering the influence of global slenderness. In this study, only the Method B is examined. According to the Method B, Eqs (8) and (9) can be used to calculate the interaction factors k_{EC3} for members with Class 1 or 2 sections subjected to major axis bending and minor axis bending, respectively; while Eq. (10) is used for the determination of k_{EC3} for members with Class 3 sections subjected to either axis bending. In Eqs (8)-(10), $\bar{\lambda}$ is the column global slenderness, C_{m} is the equivalent uniform moment factor and equals to unity for uniform moment gradient as investigated in the present study, and the subscripts 'y' and 'z' represent bending in major and minor axis, respectively.

$$k_{\mathrm{EC3,y}}=C_{\mathrm{my}}\left(1+\left(\bar{\lambda}_{\mathrm{y}}-0.2\right)\frac{N_{\mathrm{Ed}}}{N_{\mathrm{b,Rd}}}\right)\leq C_{\mathrm{my}}\left(1+0.8\frac{N_{\mathrm{Ed}}}{N_{\mathrm{b,Rd}}}\right) \tag{8}$$

$$k_{\mathrm{EC3,z}}=C_{\mathrm{mz}}\left(1+\left(2\bar{\lambda}_{\mathrm{z}}-0.6\right)\frac{N_{\mathrm{Ed}}}{N_{\mathrm{b,Rd}}}\right)\leq C_{\mathrm{mz}}\left(1+1.4\frac{N_{\mathrm{Ed}}}{N_{\mathrm{b,Rd}}}\right) \tag{9}$$

$$k_{\mathrm{EC3}}=C_{\mathrm{m}}\left(1+0.6\bar{\lambda}\frac{N_{\mathrm{Ed}}}{N_{\mathrm{b,Rd}}}\right)\leq C_{\mathrm{m}}\left(1+0.6\frac{N_{\mathrm{Ed}}}{N_{\mathrm{b,Rd}}}\right) \tag{10}$$

The experimental and numerical results are normalised by EC3 predictions and the ratios of N_u/N_{EC3} are plotted against the angle parameter θ, as shown in Figs 10 and 11 for beam-columns subject to compression plus minor axis bending and compression plus major axis bending, respectively. It can be seen from Figs 10 and 11 that the use of buckling curves 'b' and 'a' for HSS welded I-section columns buckling about the minor axis and major axis, respectively, yields accurate predictions of column buckling resistances (i.e. the EC3 predictions for specimens where the compression is dominant show less conservative compared to those where bending effects are dominant)), confirming the suitability of using higher buckling curves for HSS welded I-section column buckling design [26,27,29].

It can be seen from Figs 10 and 11 that the S960 members generally have slightly higher normalised resistances than those of S690 members, which may be attributed to the fact that the S960 members have a reduced relative influence of residual stresses (see Fig. 8) and are less sensitive to the geometric imperfections compared to the S690 members. The more conservative nature of EC3 for S960 members than S690 members is also statistically shown in Tables 5 and 6, where the mean values and coefficients of variation (COV) of N_u/N_{EC3} for the two different HSS grades are provided. For members subjected to compression plus minor axis bending, the EC3 design approach generally yields scattered and conservative predictions though a number of data points, especially for whose bending moment is dominant, lie on the unsafe side. The data points, however, follow a tighter trend for beam-column specimens under major axis bending plus compression, with generally an increasing level of conservatism with decreasing θ, as illustrated in Fig. 11. The EC3 design formulae lead to unduly conservative predictions for beam-columns with Class 3 cross-sections, especially when their bending effects are dominant. This can be attributed mainly to the undue conservatism of EC3 in the prediction of Class 3 cross-sections in bending by limiting their bending resistances to the elastic moment resistance M_{el}. This conservatism is more pronounced for beam-columns under compression plus minor axis bending as only the extreme fibres at the compression flange tips are allowed to attain the yield stress, which ignores significantly the partial spread of plasticity. This finding confirms the suggestion in [40] that a linear transition from M_{pl} to M_{el} with increasing plate slenderness should be adopted for determining the cross-sectional bending resistances of Class 3 cross-sections. In general, the EC3 design approach provides scattered and conservative strength predictions for HSS welded I-section beam-columns, owing to the inaccurate cross-sectional bending resistance predictions and, consequently, inaccurate EC3 interaction curves.

4.2 American Specification AISC 360-16 (AISC)

Similar to EC3, the American Specification AISC 360-16 [36] for the design of HSS welded I-section beam-columns follows the same procedure as for their normal strength steel counterparts. The beam-column interaction formulae specified in AISC 360-16 [36] are given in Eqs (11) and (12), where N_{Ed} is the design axial force, N_c is the column buckling resistance, M_{Ed} is the applied end moment, $M_{AISC,Rd}$ is the cross-sectional bending resistance and α is the moment amplification factor that accounts for the second-order effect in beam-columns. α is equal to 1-N_{Ed}/N_{cr}, where N_{cr} is the elastic critical axial load for the relevant column buckling mode.

$$\frac{N_{Ed}}{N_c}+\frac{8}{9\alpha}\left(\frac{M_{Ed}}{M_{AISC,Rd}}\right)\leq 1,\ \text{for}\ \frac{N_{Ed}}{N_c}\geq 0.2 \tag{11}$$

$$\frac{N_{Ed}}{2N_c}+\frac{1}{\alpha}\left(\frac{M_{Ed}}{M_{AISC,Rd}}\right)\leq 1\ ,\ \text{for}\ \frac{N_{Ed}}{N_c}< 0.2 \tag{12}$$

The column buckling resistance N_c is determined using a single buckling curve according to Section E3 of AISC 360-16 [36]. For the determination of the cross-sectional bending resistance $M_{AISC,Rd}$, the plastic moment capacity M_{pl} is adopted for compact cross-sections (i.e, equivalent to Class 1 and 2 cross-sections in EC3), whereas the effect of the partial spread of plasticity is considered in determining the cross-sectional bending resistance $M_{AISC,Rd}$ for non-slender sections (i.e. equivalent to Class 3 cross-sections in EC3).

The accuracy of the AISC design approach is evaluated through comparisons of the test and FE results with the unfactored AISC resistance predictions N_{AISC}, as illustrated in Figs 12 and 13 for loading cases of compression plus minor axis bending and compression plus major axis bending, respectively. It can be seen from Figs 12 and 13 that the normalised test and FE data points N_u/N_{AISC} follow a tighter trend for both loading cases compared to the EC3 predictions, revealing improved accuracy and consistency of AISC over EC3. This is also revealed quantitatively by the statistical results summarised in Tables 5 and 6. However, there are still a large number of data points lying on the unsafe side, indicating the need for developing more rational and accurate design rules for HSS welded I-section beam-columns.

4.3 The Continuous Strength Method (CSM)

A new design approach based on the Continuous Strength Method (CSM) is proposed in this section for the design of HSS welded I-section beam-columns. The CSM is a deformation based design approach that replaces the concept of cross-section classification with a continuous relationship between cross-section slenderness and deformation capacity, enabling the effective utilisation of material strain hardening as well as the partial spread of plasticity and, thus, providing more accurate and consistent cross-section resistance predictions. The CSM is a ground-up design approach that started from the design of stainless steel cross-sections [1,2,4] and now has been extended to the design of carbon steel cross-sections [11-15], indeterminate structures [16,17], composite structures [41] as well as structures in fire [42]. The new proposed design formula for HSS welded I-section beam-columns follows the general format employed in EC3 [34,35], but adopts more accurate end points (i.e. flexural buckling resistance and cross-sectional bending resistance) and the accordingly updated interaction factors, as given in Eq. (13).

$$\frac{N_{\mathrm{Ed}}}{N_{\mathrm{b,Rd}}}+k_{\mathrm{csm}}\frac{M_{\mathrm{Ed}}}{M_{\mathrm{csm,Rd}}}\leq 1 \tag{13}$$

The new column bucking curves (i.e. buckling curve 'a' for major axis buckling and curve 'b' for minor axis buckling for both the S690 and S960 welded I-section columns) as suggested by [26,27,29] and reconfirmed in the present study are used to determine the flexural buckling resistance $N_{\mathrm{b,Rd}}$ in Eq. (13). The CSM cross-section bending resistance $M_{\mathrm{csm,Rd}}$, which has shown to provide more accurate and consistent resistance predictions than the current codified design provisions [11,12], is utilised in the new proposed design equation Eq. (13) as the pure bending end point. The quad-linear material model, developed by Yun and Gardner [19] and included in prEN 1993-1-14 [43], was utilised as the CSM material model for S690 steel to represent its stress-strain response which is generally characterised by a succession of a linear elastic portion up to a well-defined yield point, a yield plateau and then some strain hardening, as typically shown in Fig. 1(a). While for S960 steel which normally has a rounder stress-strain response with no sharply defined yield point, as shown in Fig. 1(b), the bilinear material model proposed in [12] was employed as the CSM material model. In accordance with the adopted CSM material model, the equations for calculating the CSM cross-section bending resistance $M_{\mathrm{csm,Rd}}$ are given by Eqs (14) and (15) [11] for non-slender I-sections made of S690 steel and by Eq. (16) [12] for non-slender I-sections made of S960 steel, in which W_{pl} is the plastic section modulus, W_{el} is the elastic section modulus, E_{sh}, ε_{csm} and ε_{sh} are the strain-hardening modulus, the CSM strain that a cross-section can sustain prior to local buckling and the strain hardening strain where the material yield plateau ends and the strain hardening initiates, respectively, and the coefficients α and β are taken as 1.2 and 0.05 for I-sections under minor axis bending, respectively, and 2 and 0.1 for major axis bending, respectively. More details regarding the derivation of Eqs (14)-(16) and the parameters thereof can be found in [11,12,19].

$$M_{\mathrm{csm,Rd}} = \frac{W_{\mathrm{pl}} f_{\mathrm{y}}}{\gamma_{\mathrm{M0}}}\left[1-\left(1-\frac{W_{\mathrm{el}}}{W_{\mathrm{pl}}}\right)\Big/\left(\frac{\varepsilon_{\mathrm{csm}}}{\varepsilon_{\mathrm{y}}}\right)^{\alpha}\right], \text{ for S690 sections with } \varepsilon_{\mathrm{y}} < \varepsilon_{\mathrm{csm}} \le \varepsilon_{\mathrm{sh}} \tag{14}$$

$$M_{\mathrm{csm,Rd}} = \frac{W_{\mathrm{pl}} f_{\mathrm{y}}}{\gamma_{\mathrm{M0}}}\left[1-\left(1-\frac{W_{\mathrm{el}}}{W_{\mathrm{pl}}}\right)\Big/\left(\frac{\varepsilon_{\mathrm{csm}}}{\varepsilon_{\mathrm{y}}}\right)^{\alpha} + \beta\left(\frac{\varepsilon_{\mathrm{csm}}-\varepsilon_{\mathrm{sh}}}{\varepsilon_{\mathrm{y}}}\right)^{2}\frac{E_{\mathrm{sh}}}{E}\right], \text{ for S690 sections with } \varepsilon_{\mathrm{csm}} > \varepsilon_{\mathrm{sh}} \tag{15}$$

$$M_{\mathrm{csm,Rd}} = \frac{W_{\mathrm{pl}} f_{\mathrm{y}}}{\gamma_{\mathrm{M0}}}\left[1+\frac{E_{\mathrm{sh}}}{E}\frac{W_{\mathrm{el}}}{W_{\mathrm{pl}}}\left(\frac{\varepsilon_{\mathrm{csm}}}{\varepsilon_{\mathrm{y}}}-1\right)-\left(1-\frac{W_{\mathrm{el}}}{W_{\mathrm{pl}}}\right)\Big/\left(\frac{\varepsilon_{\mathrm{csm}}}{\varepsilon_{\mathrm{y}}}\right)^{\alpha}\right], \text{ for S960 sections with } \varepsilon_{\mathrm{csm}} > \varepsilon_{\mathrm{y}} \tag{16}$$

Based on the more accurate end points, a new interaction factor k_{csm} is also proposed following the same procedure used in [7,44,45]. The expression for determining the new interaction factor k_{csm} is given by Eq. (17), which is a function of the column slenderness $\bar{\lambda}$ and the normalised axial load $N_{Ed}/N_{b,Rd}$. In Eq. (17), D_1, D_2 and D_3 are dimensionless coefficients that are determined by fitting Eq. (17) to the dataset of the back-calculated interaction factor $k_{csm,FE}$ (i.e. calculated by rearranging Eq. (13)) based on the FE results, as given in Table 7. Figs 14-17 show the comparisons between the FE back-calculated $k_{csm,FE}$ and the proposed k_{csm} using the fitted expression Eq. (17) for S690 and S960 members under different loading scenarios. In

Figs 14-17, both the $k_{\mathrm{csm,FE}}$ and k_{csm} are plotted against the normalised axial load $N_{\mathrm{Ed}}/N_{\mathrm{b,Rd}}$ for different column slenderness $\bar{\lambda}$ ranging from 0.3 to 2.5. It can be seen from Figs 14-17 that the proposed k_{csm} follow the general trend of the FE back-calculated $k_{\mathrm{csm,FE}}$ and lie above the $k_{\mathrm{csm,FE}}$ for all investigated ranges of column slenderness $\bar{\lambda}$ and axial load ratios $N_{\mathrm{Ed}}/N_{\mathrm{b,Rd}}$, indicating that Eq. (17) provides an accurate yet conservative representation of the $k_{\mathrm{csm,FE}}$.

$$k_{\mathrm{csm}} = 1 + D_1\left(\bar{\lambda} - D_2\right)\frac{N_{\mathrm{Ed}}}{N_{\mathrm{b,Rd}}} \text{ but } k_{\mathrm{csm}} \leq 1 + D_1\left(D_3 - D_2\right)\frac{N_{\mathrm{Ed}}}{N_{\mathrm{b,Rd}}} \tag{17}$$

The accuracy of the proposed design approach for HSS welded I-section beam-columns is evaluated using the test and FE results, as shown in Figs 18 and 19 where the normalised test and FE resistances $N_{\mathrm{u}}/N_{\mathrm{csm}}$ are plotted against the angle parameter θ for beam-columns under compression plus minor axis bending and compression plus major axis bending, respectively. It is shown from Figs 18 and 19 that the proposed design approach provides significantly improved resistance predictions than the current codified design provisions; the improvement is particularly pronounced for specimens whose bending effects are dominant (i.e. specimens with small values of θ) owing primarily to the utilisation of CSM for the calculation of the cross-sectional bending resistance, which provides an improved level of accuracy and consistency over the codified design approaches. The comparison results are also statistically summarised in Tables 5 and 6 for specimens subjected to compression plus minor axis bending and compression plus major axis bending, respectively, revealing that the proposed CSM based design approach provides safe-sided resistance predictions and is substantially more accurate and less scattered than the current codified design methods. The improvement of the proposed CSM-based method is resulted from (1) the utilization of the recently proposed column buckling curves [26,27,29] with improved accuracy to determine the high strength steel welded

I-section column buckling resistances (i.e. column buckling end points); (2) the adoption of the Continuous Strength Method (CSM) to determine the cross-sectional bending resistances of welded I-sections (i.e. bending end points) [11,12] and (3) the derivation of new interaction curves for high strength steel welded I-section beam-columns, which are anchored to these more accurate end points.

4.4 Reliability analysis

To evaluate the reliability of the design rules set out in EC3 [34,35] and AISC 360-16 [36], as well as the proposed CSM based design approach, a careful reliability analysis was performed in accordance with the standard procedure set out in Annex D of EN 1990 [46]. Note that the beam-column design rules set out in AISC 360-16 [36] were also assessed using the EN 1990 [46] reliability assessment procedure to facilitate direct comparison among different design methods, though the AISC 360-16 [36] has its own reliability assessment approach.

In the reliability analysis, the COV of the cross-section area V_A is taken as 0.03, as recommended by Byfield and Nethercot [47]. The COV of material yield strength V_{fy} and the material overstrength factor are taken as 0.06 and 1.15, respectively, for S690, and 0.04 and 1.04, respectively, for S960, as suggested by Feldmann et al. [48]. Detailed information regarding the reliability analysis procedure can be found in Annex D of EN 1990 [46] and Afshan et al. [49], while only essential reliability analysis results are reported herein, as given in Tables 8 and 9 for specimens subjected to compression plus minor axis bending and compression plus major axis bending, respectively. In Tables 8 and 9, b is the mean correction factor, k_d is the design fractile factor modelled based on the Student T-distribution [50], V_δ is the COV of the test and FE resistance relative to the predictions calculated from the design equation, and γ_{M1} is the partial safety factor which has a target value of unity [34,35]. Note that the mean correction factor b is calculated using Eq. (18) instead of the least-squares method suggested in EN 1990 [46], where n is the number of experimental and FE data, r_e is the experimental or FE failure load, and r_t is the corresponding theoretical (predicted) resistance determined from different design methods. This approach prevents the determined value of b from being biased towards the experimental and FE data with higher ultimate resistances [12,51].

$$b = \frac{1}{n}\sum_{i=1}^{n}\frac{r_{e,i}}{r_{t,i}} \tag{18}$$

As shown in Tables 8 and 9, the required partial safety factors for the proposed CSM-based design approach are equal to or slightly higher than the target value of unity for different steel grades under different cases, but generally lower than the corresponding values for the EC3 and AISC design approaches. Even lower required partial safety factors can be obtained if the reliability analysis was performed on the sub-sets of the test and FE data for S960 specimens based on the cross-section classes. Therefore, the EC3 suggested partial safety factor γ_{M1} of unity for beam-column design is deemed appropriate to the proposed CSM based design approach.

5. Conclusions

An in-depth numerical study into the structural behaviour and design of HSS welded I-section beam-columns under compression plus uniaxial bending is carried out in the present study. Finite element models were developed and validated against existing experimental data on S690 and S960 welded I-section columns and beam-columns [27,32]. On the basis of the validated FE models, a parametric study consisting of 1728 numerical models was performed to generate additional structural performance data, which were utilised to appraise the accuracy of both the codified and proposed beam-column design rules. The following conclusions have been made:

- Both EC3 and AISC design approaches provide somewhat inaccurate and scattered resistance predictions for HSS welded I-section beam-columns;
- The proposed CSM-based design approach is shown to provide more accurate and consistent resistance predictions than the existing codified design methods;
- The reliability analysis confirms that the partial safety factor of unity recommended in EC3 is also applicable for use in the proposed CSM-based design approach.

It should be noted that though the CSM based design approach was underpinned by test and FE data on S690 and S960 welded I-section beam-columns subjected to uniaxial bending plus compression, its concept can be extended to the design of structural members made of other cross-section shapes and/or subjected to more complicated loading conditions, which requires further research in this area. In addition, extending the CSM-based method to the design of beam-columns with slender cross-sections is also required in future work.

References

[1]. L. Gardner, The continuous strength method, Proc. Inst. Civ. Eng. Struct. Build. 161(3) (2008) 127–133.

[2]. S. Afshan, L. Gardner, The continuous strength method for structural stainless steel design, Thin-Walled Struct. 68 (2013) 42–49.

[3]. O. Zhao, S. Afshan, L. Gardner, Structural response and continuous strength method design of slender stainless steel cross-sections, Eng. Struct. 140 (2017) 14–25.

[4]. L. Gardner, Stability and design of stainless steel structures–Review and outlook, Thin-Walled Struct. 141 (2019) 208-216.

[5]. A.S.J. Foster, L. Gardner, Stability of steel beams using the continuous strength method, Thin-Walled Struct. 100 (2016) 1–13.

[6]. Y.D. Bu, L. Gardner, Laser-welded stainless steel I-section beam-columns: Testing, simulation and design, Eng. Struct. 179 (2019) 23–26.

[7]. L. Yang, M.H. Zhao, L. Gardner, K.Y. Ning, J. Wang, Member stability of stainless steel welded I-section beam-columns, J. Constr. Steel Res. 155 (2019) 33–45.

[8]. M. Su, B. Young, L. Gardner, Continuous strength method for aluminium alloy structures, Adv. Mat. Res. 742 (2013) 70–75.

[9]. M. Su, B. Young, L. Gardner, The continuous strength method for the design of aluminium alloy structural elements, Eng. Struct. 122 (2016) 338–348.

[10]. M. Ashraf, B. Young, Design formulations for non-welded and welded aluminium columns using continuous strength method, Eng. Struct. 33(12) (2011) 3197–3207.

[11]. X. Yun, L. Gardner, N. Boissonnade, The continuous strength method for the design of hot-rolled steel cross-sections, Eng. Struct. 157 (2018) 179–191.

[12]. X. Yun, L. Gardner, The continuous strength method for the design of cold-formed steel non-slender tubular cross-sections, Eng. Struct. 175 (2018) 549-564.

[13]. X. Yun, L. Gardner, N. Boissonnade, Ultimate capacity of I-sections under combined loading–Part 1: Experiments and FE model validation, J. Constr. Steel Res. 147 (2018) 408-421.

[14]. X. Yun, L. Gardner, N. Boissonnade, Ultimate capacity of I-sections under combined loading–Part 2: Parametric studies and CSM design, J. Constr. Steel Res. 148 (2018) 265-274.

[15]. X. Yun, Z.X. Wang, L. Gardner, Structural performance and design of hot-rolled steel SHS and RHS under combined axial compression and bending, Structures 27 (2020) 1289-1298.

[16]. L. Gardner, X. Yun, A. Fieber, L. Macorini, Steel design by advanced analysis: material modeling and strain limits, Engineering 5(2) (2019) 243-249.

[17]. X. Yun, L. Gardner, Numerical modelling and design of hot-rolled and cold-formed steel continuous beams with tubular cross-sections, Thin-Walled Struct. 132 (2018) 574-584.

[18]. X. Lan, J. Chen, T.M. Chan, B. Young, The continuous strength method for the design of high strength steel tubular sections in compression. Eng. Struct. 162 (2018) 177-187.

[19]. X. Yun, L. Gardner, Stress-strain curves for hot-rolled steels, J. Constr. Steel Res. 133 (2017) 36-46.

[20]. J.L. Ma, T.M. Chan, B. Young, Experimental Investigation on Stub-Column Behavior of Cold-Formed High-Strength Steel Tubular Sections, J. Struct. Eng. 142(5) (2016) 04015174.

[21]. G. Shi, W.J. Zhou, Y. Bai, C.C. Lin, Local buckling of 460 MPa high strength steel welded section stub columns under axial compression, J. Constr. Steel Res. 100 (2014) 60–70.
[22]. L. Gao, H.C. Sun, F.N. Jin, H.L. Fan, Load-carrying capacity of high-strength steel box-sections I: Stub columns, J. Constr. Steel Res. 65(4) (2009) 918–924.
[23]. K.J.R. Rasmussen, G.J. Hancock, Plate slenderness limits for high strength steel sections, J. Constr. Steel Res. 23(1–3) (1992) 73–96.
[24]. F. Zhou, L.W. Tong, Y.Y. Chen, Experimental and numerical investigations of high strength steel welded H-section columns, Int. J. Steel Struct. 13(2) (2013) 209-218.
[25]. J. Wang, L. Gardner, Flexural buckling of hot-finished high-strength steel SHS and RHS columns, J. Struct. Eng. 143(6) (2017) 04017028.
[26]. H.Y. Ban, G. Shi, Y.J. Shi, Y.Q. Wang, Overall buckling behavior of 460 MPa high strength steel columns: Experimental investigation and design method, J. Constr. Steel Res. 74 (2012) 140–150.
[27]. H.Y. Ban, G. Shi, Y.J. Shi, M.A. Bradford, Experimental investigation of the overall buckling behaviour of 960 MPa high strength steel columns, J. Constr. Steel Res. 88 (2013) 256–266.
[28]. T.J. Li, G.Q. Li, S.L. Chan, Y.B. Wang, Behavior of Q690 high-strength steel columns: Part 1: Experimental investigations, J. Constr. Steel Res. 123 (2016) 18–30.
[29]. T.J. Li, S.W. Liu, G.Q. Li, S.L. Chan, Y.B. Wang, Behavior of Q690 high-strength steel columns: Part 2: Parametric study and design recommendations, J. Constr. Steel Res. 122 (2016) 379–394.
[30]. T.Y. Ma, X. Liu, Y.F. Hu, K.F. Chung, G.Q. Li, Structural behaviour of slender columns of high strength S690 steel welded H-sections under compression, Eng. Struct. 157 (2018) 75–85.
[31]. B. Yang, L. Shen, S.B. Kang, M. Elchalakani, S.D. Nie, Load bearing capacity of welded Q460GJ steel H-columns under eccentric compression, J. Constr. Steel Res. 143 (2018) 320–330.
[32]. T.Y. Ma, Y.F. Hu, X. Liu, G.Q. Li, K.F. Chung, Experimental investigation into high strength Q690 steel columns of welded H-sections under combined compression and bending, J. Constr. Steel Res. 138 (2017) 449–462.
[33]. T.Y. Ma, G.Q. Li, K.F. Chung, Numerical investigation into high strength Q690 steel columns of welded H-sections under combined compression and bending, J. Constr. Steel Res. 144 (2018) 119–134.

[34]. EN 1993-1-1, Eurocode 3: Design of steel Structure – Part 1–1: General rules and rules for buildings, European Committee for Standardization (CEN), Brussels, 2005.
[35]. EN 1993-1-12, Eurocode 3: Design of steel structures – Part 1-12: Additional rules for the extension of EN 1993 up to steel grades S700, European Committee for Standardization (CEN), Brussels, 2007.
[36]. ANSI/AISC 360-16, Specification for Structural Steel Buildings, American Institute of Steel Construction (AISC), Chicago, Illinois, 2016.
[37]. ABAQUS, Standard user's manual volume I–III and ABAQUS CAE manual. Version 6.14, Hibbitt, Karlsson and Sorensen Inc, 2014.
[38]. EN 1993-1-5, Eurocode 3: Design of steel structures – Part 1-5: Plated structural elements, European Committee for Standardization (CEN), Brussels, 2006.
[39]. R.D. Ziemian, Guide to Stability Design Criteria for Metal Structures, Sixth ed., New York, John & Sons, Inc., 2010.
[40]. A. Taras, R. Greiner, H. Unterweger, Proposal for amended rules for member bucking and semi-compact cross-section design, Technical Report, Consolidated Version of Documents of the Same Title Submitted to the SC3 Evolution Group 1993–1-1, Paris, 2013.
[41]. L. Gardner, X. Yun, L. Macorini, M. Kucukler, Hot-rolled steel and steel-concrete composite design incorporating strain hardening, Structures 9 (2017) 21-28.
[42]. X. Yun, N. Saari, L. Gardner, Behaviour and design of eccentrically loaded hot-rolled steel SHS and RHS stub columns at elevated temperatures, Thin-Walled Struct. 149 (2020) 106646.
[43]. prEN 1993-1-14, Eurocode 3: Design of steel structures – Part 1-14: Design by FE analysis, European Committee for Standardization (CEN), Brussels, 2019.
[44]. R. Greiner, J. Lindner, Interaction formulae for members subjected to bending and axial compression in EUROCODE 3–the Method 2 approach, J. Constr. Steel Res. 62(8) (2006) 757-770.
[45]. R. Greiner, M. Kettler, Interaction of bending and axial compression of stainless steel members, J. Constr. Steel Res. 64(11) (2008) 1217-1224.
[46]. EN 1990, Eurocode – Basis of structural design, European Committee for Standardization (CEN), Brussels, 2002.
[47]. M.P. Byfield, D.A. Nethercot, An analysis of the true bending strength of steel beams, Proc. Inst. Civ. Eng. Struct. Build. 128(2) (1998) 188–197.

[48]. M. Feldmann, N. Schillo, S. Schaffrath, K. Virdi, T. Björk, N. Tuominen, et al., Rules on high strength steel (RUOSTE): Final Report, Publications Office of the European Union, Luxembourg, 2016.

[49]. S. Afshan, P. Francis, N.R. Baddoo, L. Gardner, Reliability analysis of structural stainless steel design provisions, J. Constr. Steel Res. 114 (2015) 293–304.

[50]. K. Law, Instabilities in structural steel elliptical hollow section members (PhD thesis) Department of Civil and Environmental Engineering, Imperial College London, UK, 2010.

[51]. X. Meng, L. Gardner, Behavior and design of normal-and high-strength steel SHS and RHS columns. J. Struct. Eng. 146(11) (2020) 04020227.

Figures:

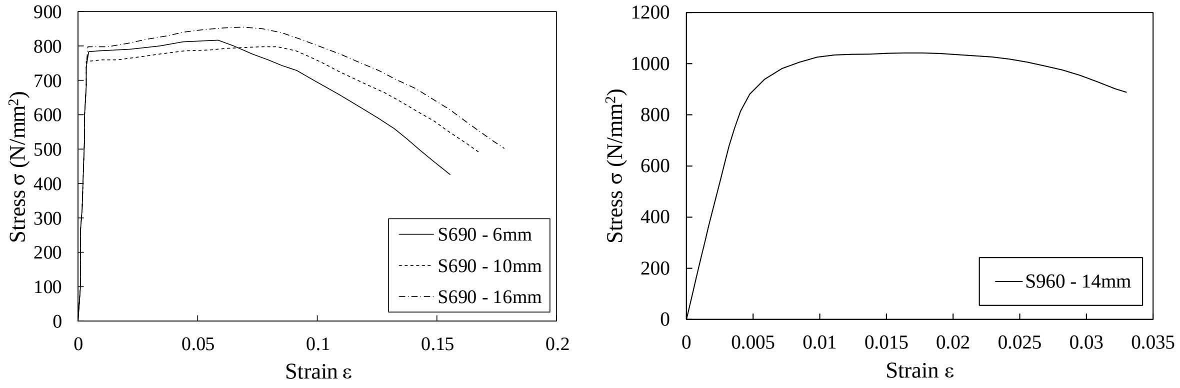

(a) S690 [32] (b) S960 [27]

Fig. 1. Engineering stress-strain curves from tensile coupon tests [27,32]

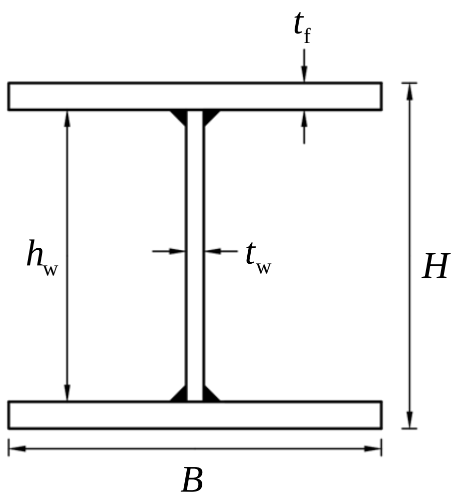

Fig. 2. Definition of symbols for HSS welded I-sections

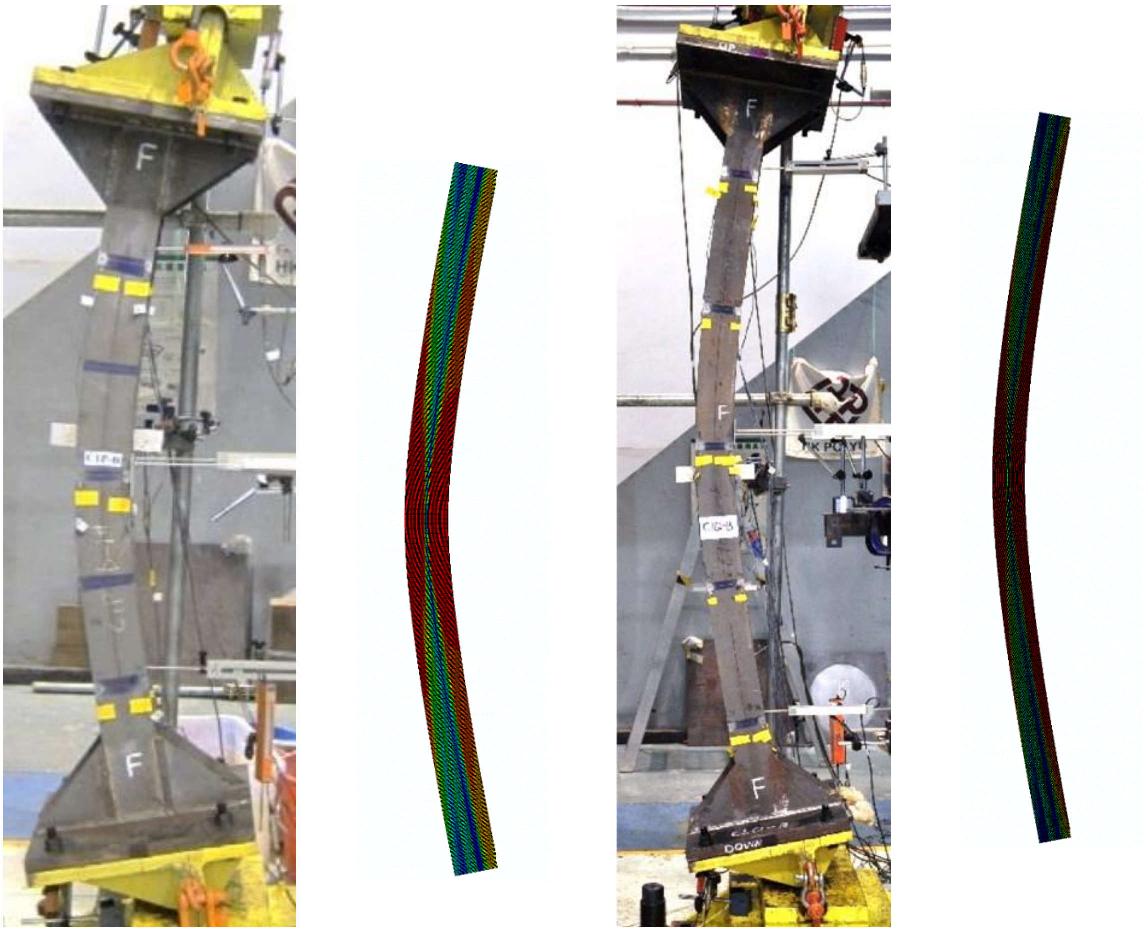

(a) EH1P - Test (b) EH1P - FE (c) EH1Q - Test (d) EH1Q - FE

Fig. 3. Comparisons of test and FE failure modes of specimens EH1P and EH1Q [32]

(a) H1-960 - Test (b) H1-960 - FE

Fig. 4. Comparison of test and FE failure modes of specimen H1-960 [27]

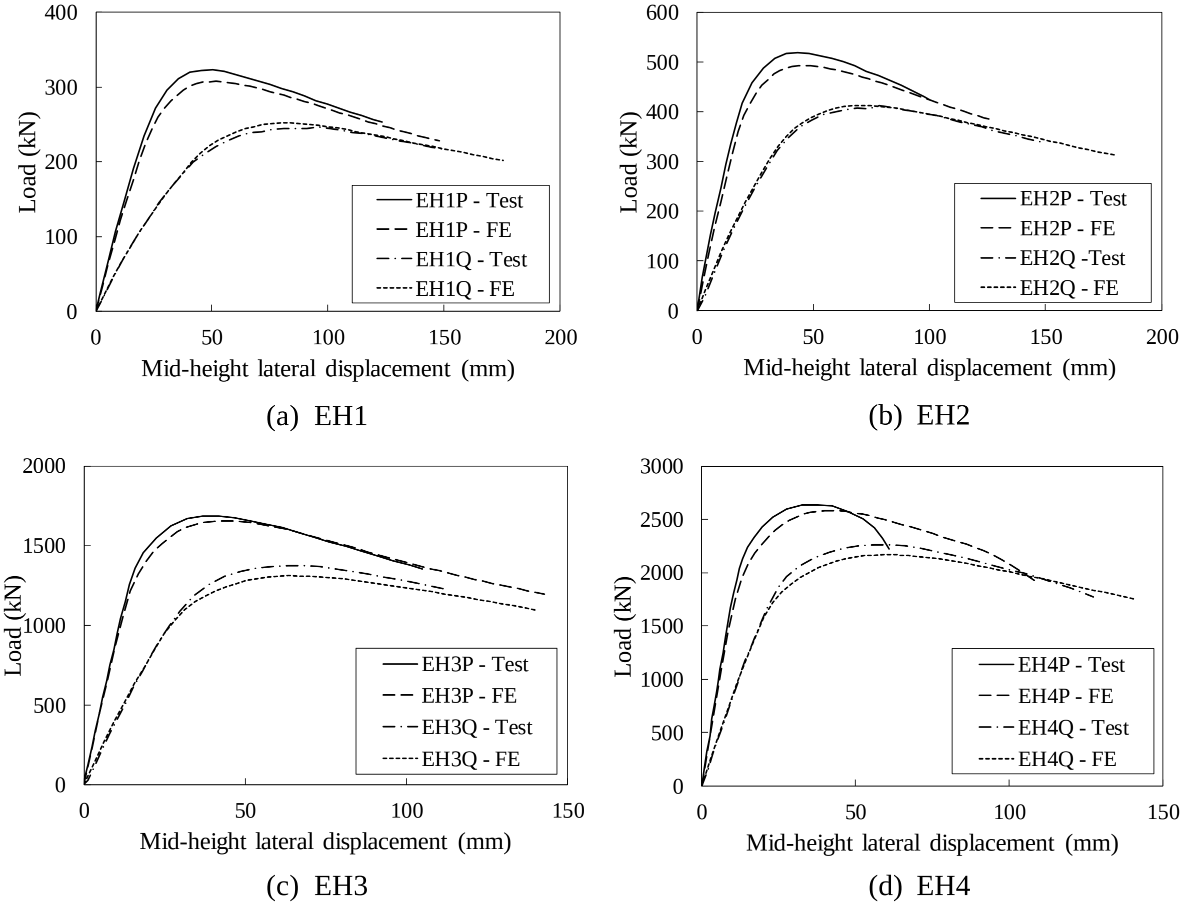

(a) EH1 (b) EH2

(c) EH3 (d) EH4

Fig. 5. Experimental and numerical load-mid-height lateral displacement curves for S690 specimens [32]

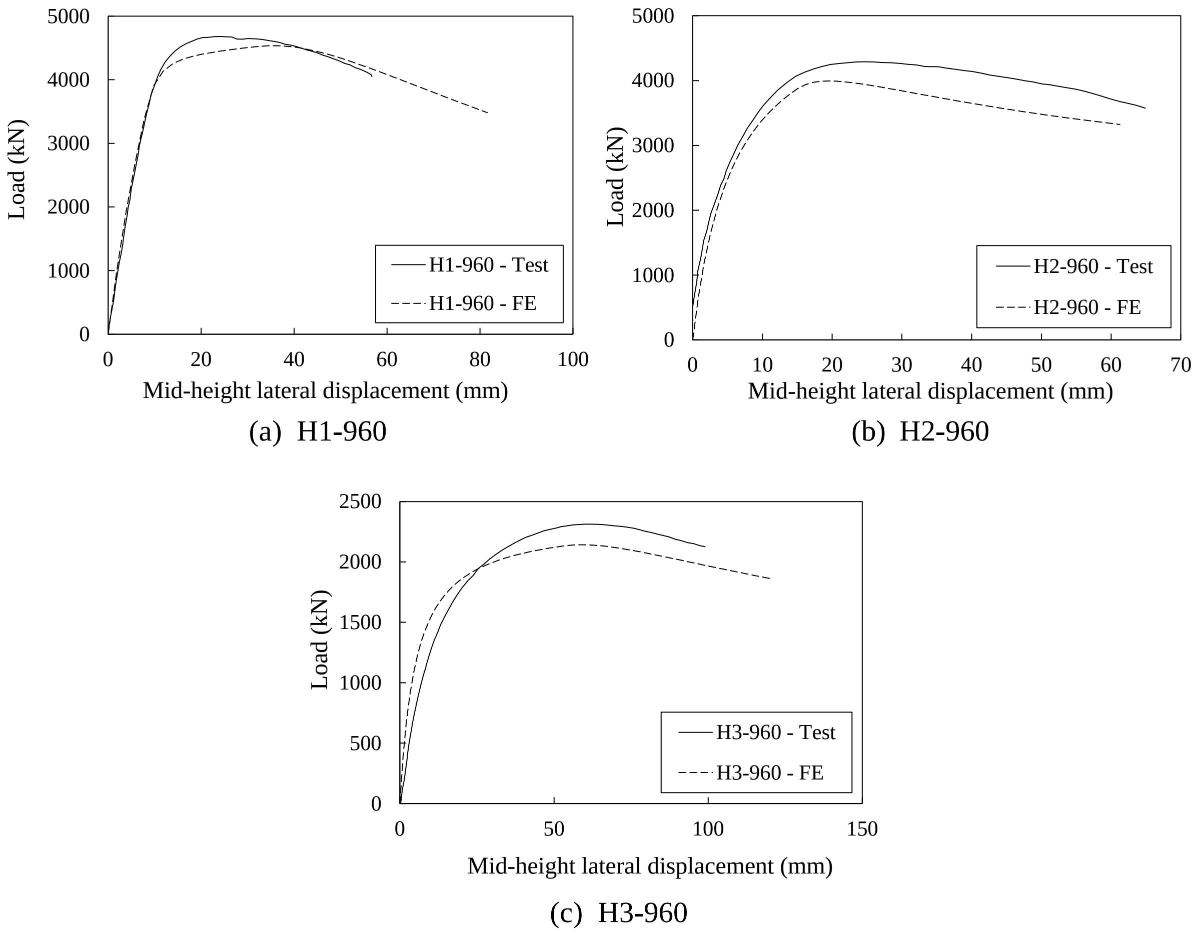

Fig. 6. Experimental and numerical load-lateral displacement curves for S960 specimens [27]

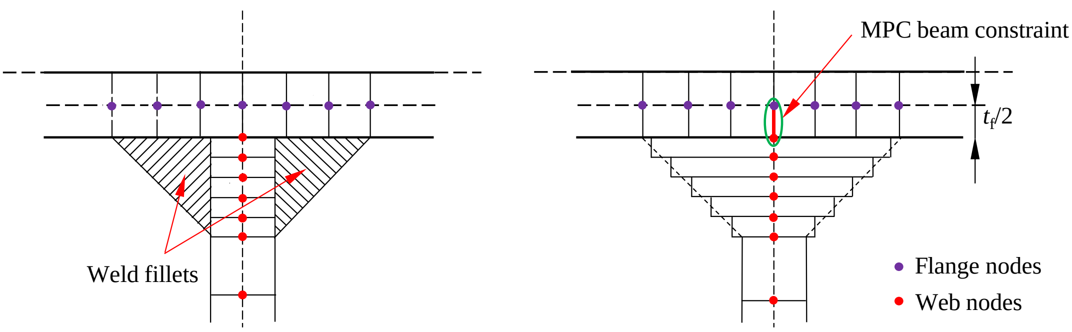

Fig. 7. Modelling of weld fillets of welded I-sections in FE models for validation purpose.

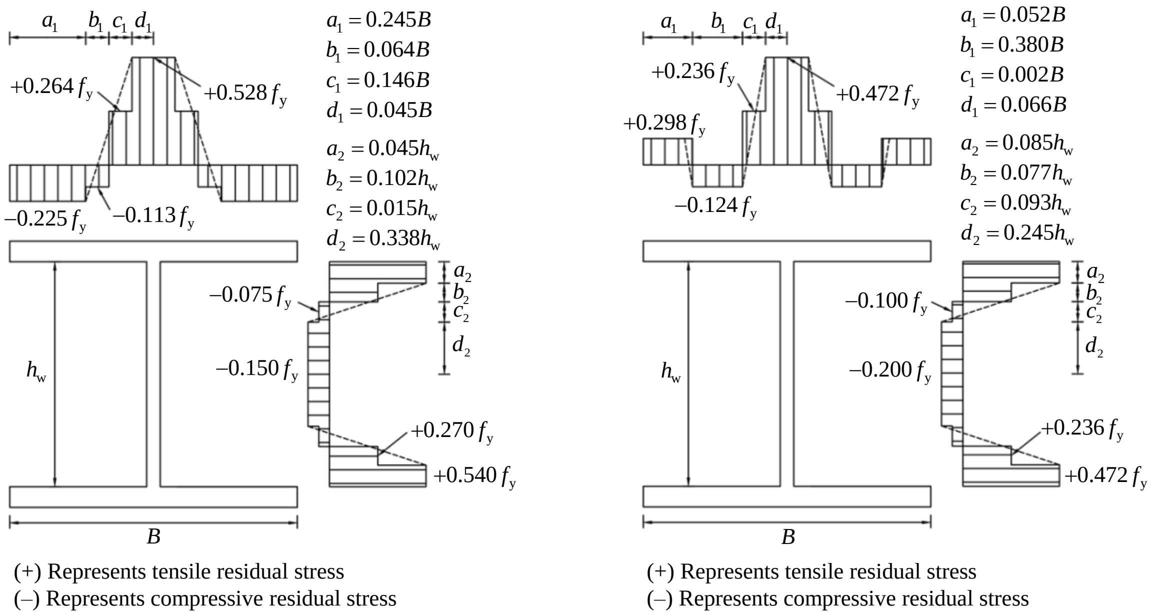

(a) S690 (b) S960

Fig. 8. Proposed residual stress pattern for HSS welded I-sections based on experimental measures [7,27,32]

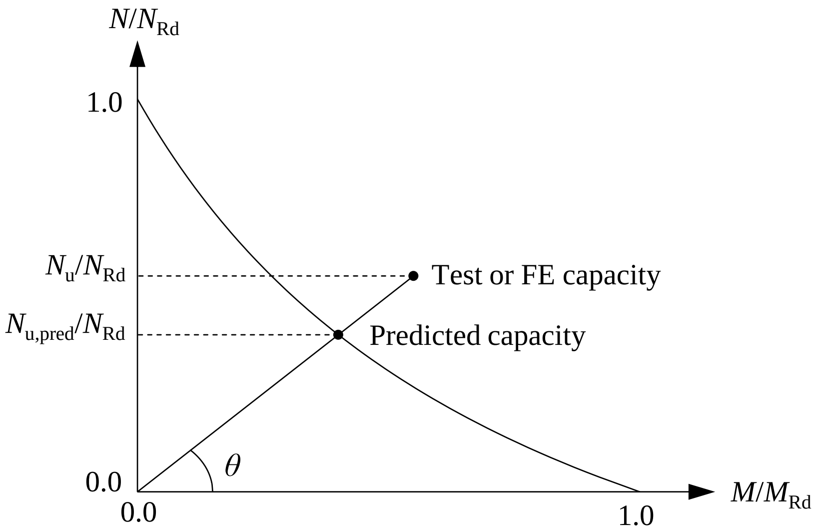

Fig. 9. Definition of θ on the axial load-moment interaction curve

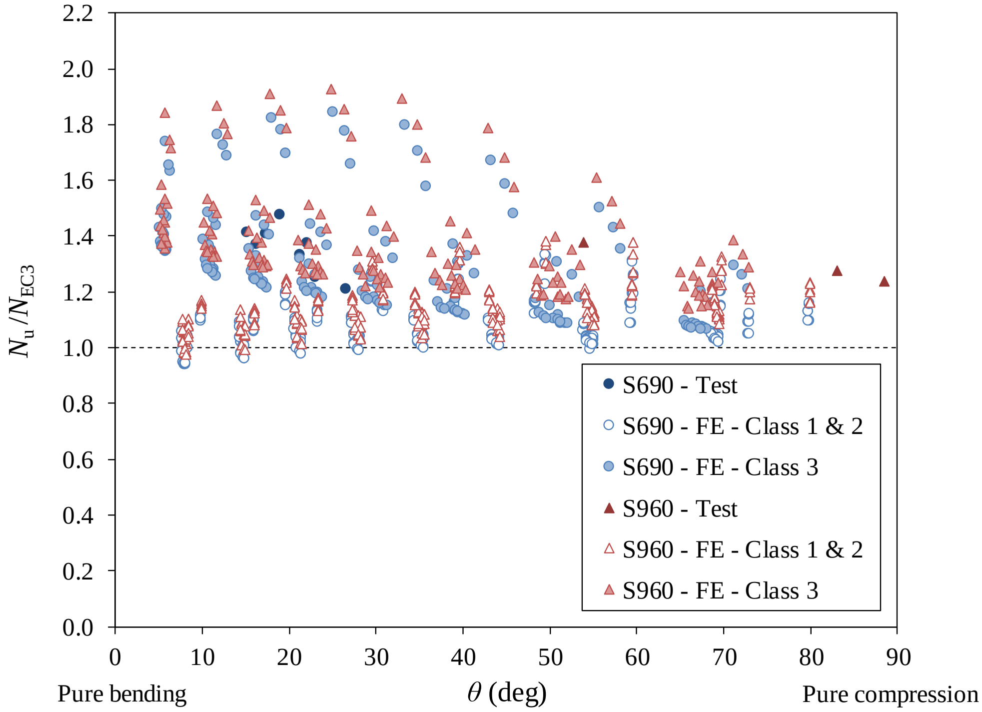

Fig. 10. Comparison of test and FE results with design resistances predicted by EC3 [34,35] for HSS welded I-sections under compression plus minor axis bending

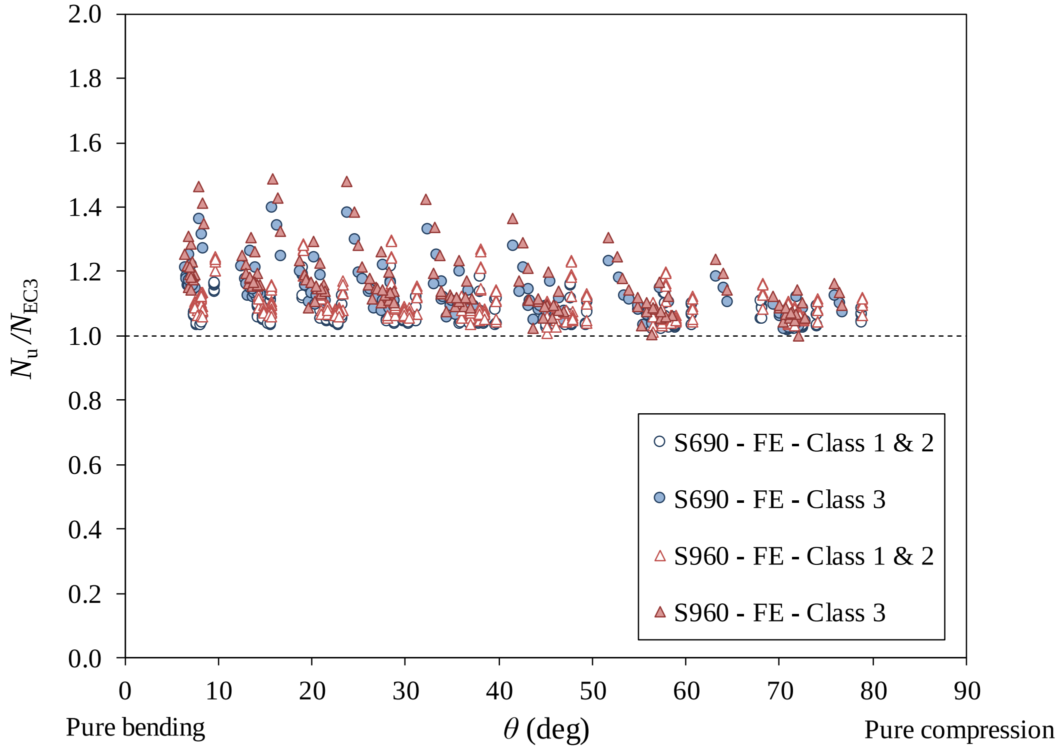

Fig. 11. Comparison of FE results with design resistances predicted by EC3 [34,35] for HSS welded I-sections under compression plus major axis bending

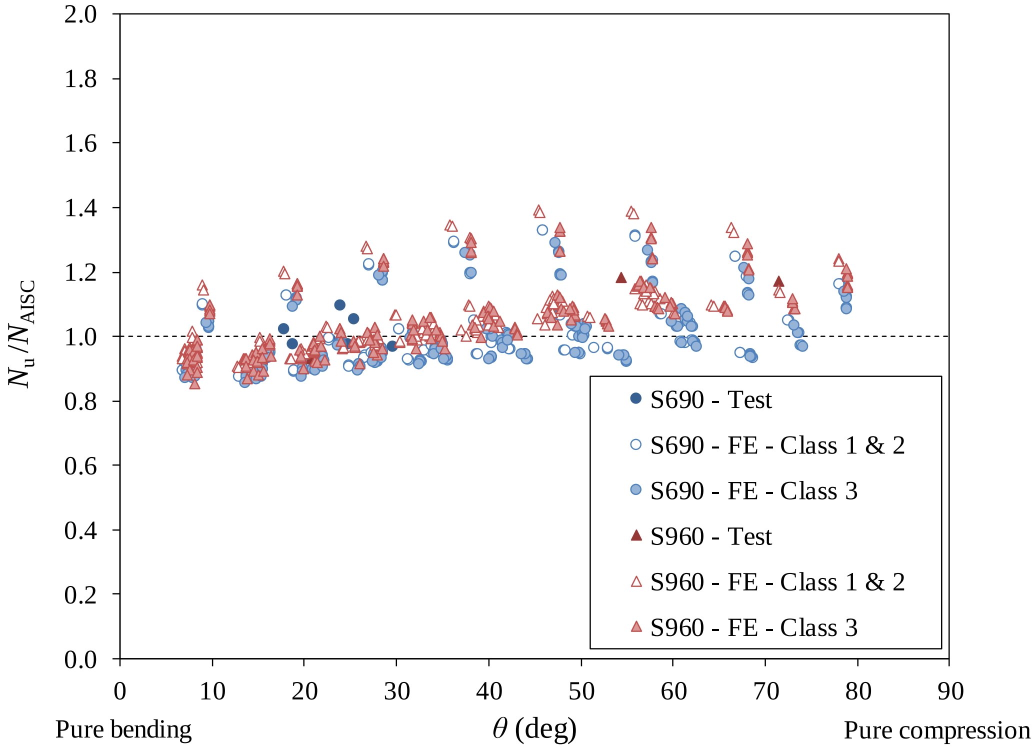

Fig. 12. Comparison of test and FE results with design resistances predicted by AISC [36] for HSS welded I-sections under compression plus minor axis bending

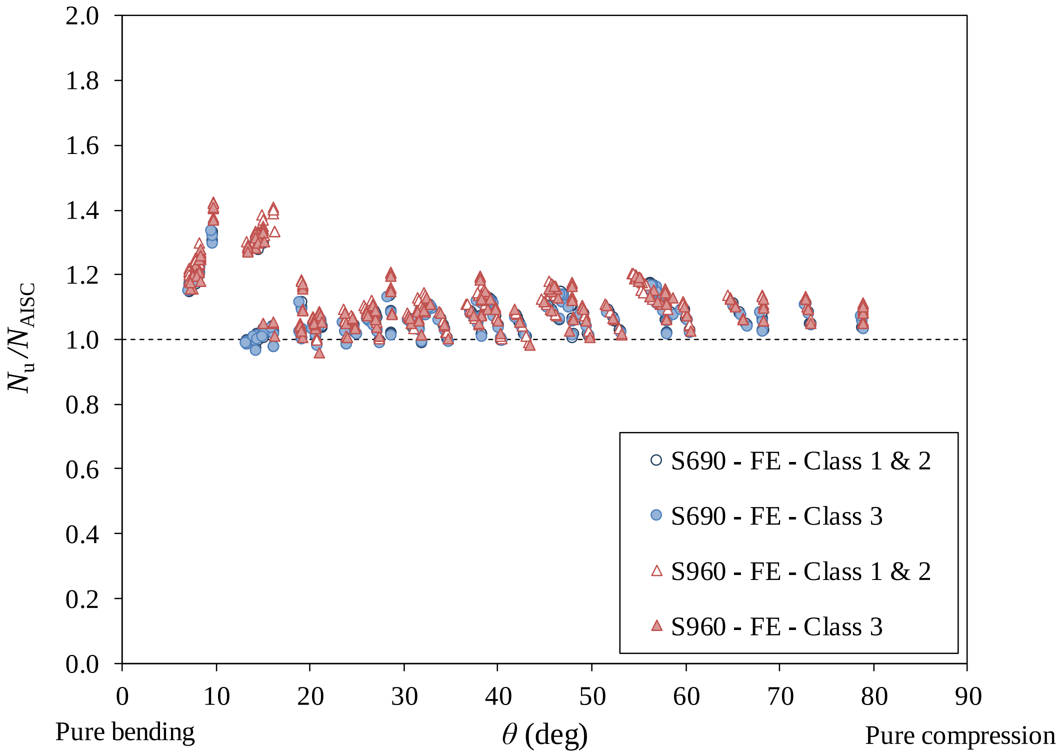

Fig. 13. Comparison of FE results with design resistances predicted by AISC [36] for HSS welded I-sections under compression plus major axis bending

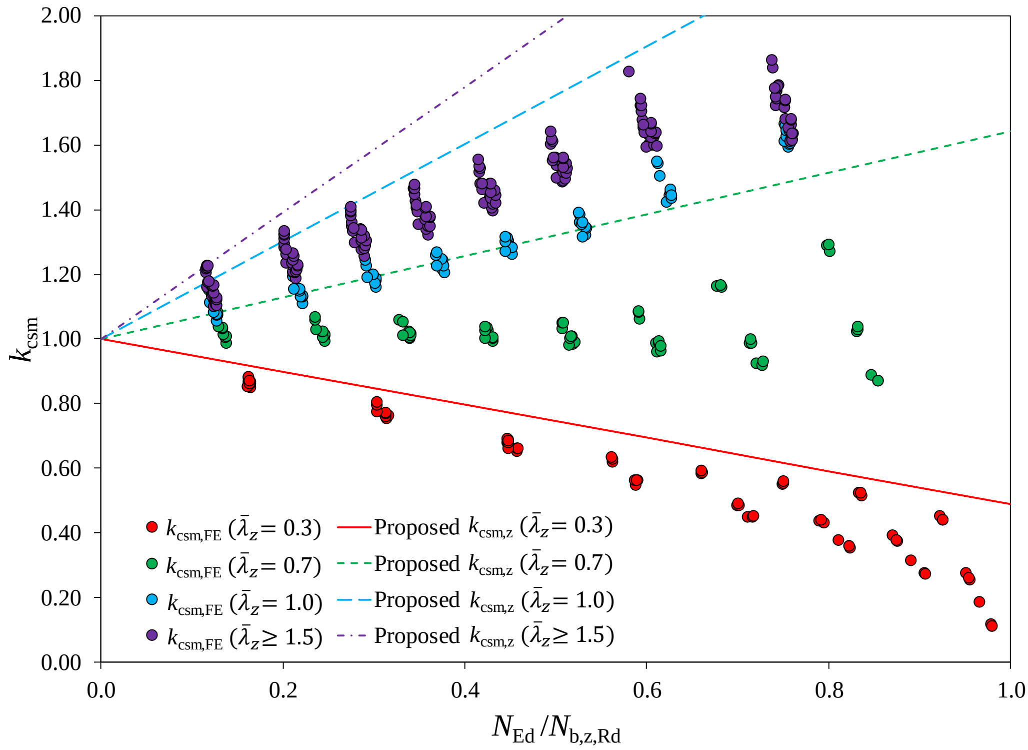

Fig. 14. Proposed CSM interaction factor for S690 welded-I section beam-columns under compression plus minor axis bending

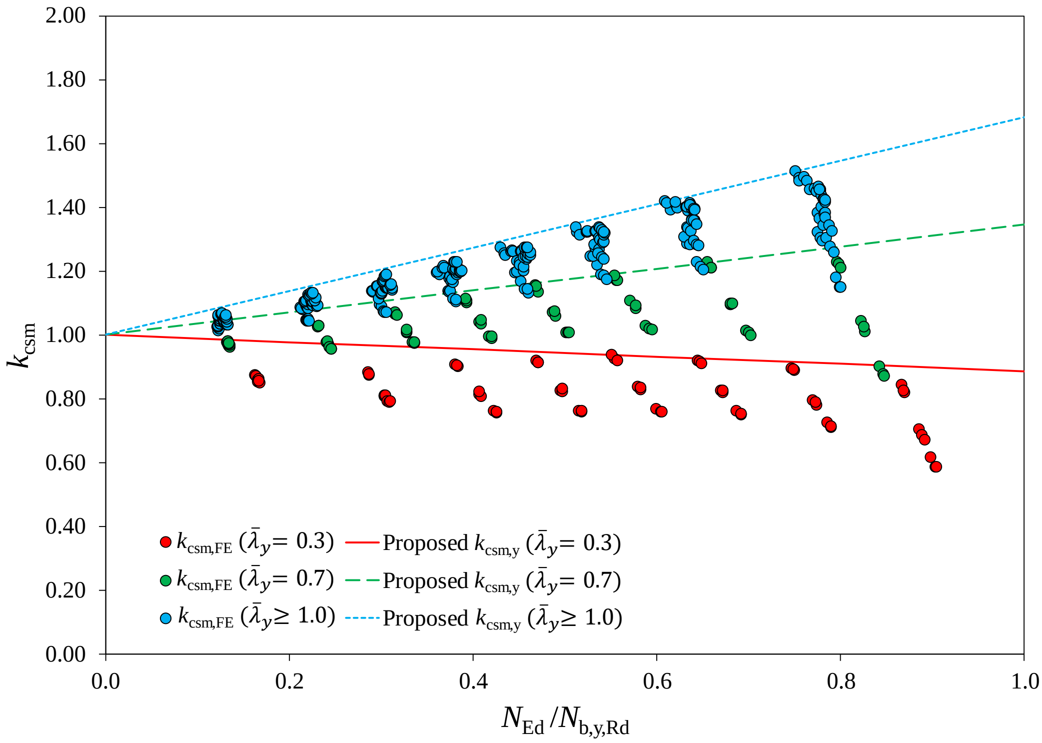

Fig. 15. Proposed CSM interaction factor for S690 welded-I section beam-columns under compression plus major axis bending

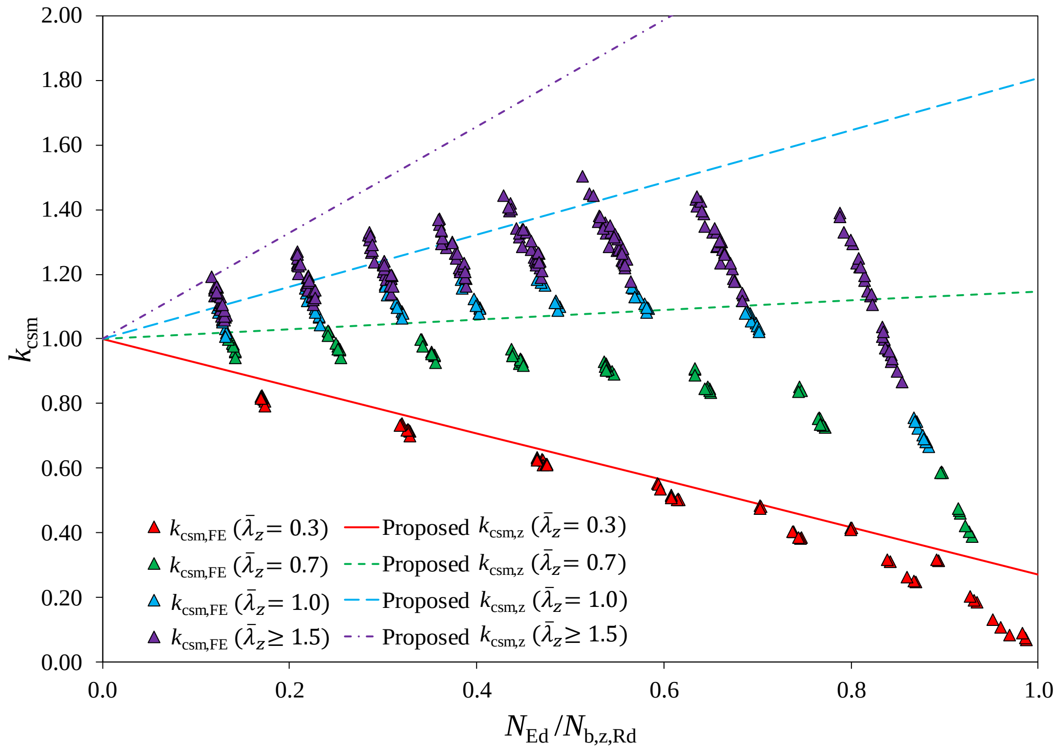

Fig. 16. Proposed CSM interaction factor for S960 welded-I section beam-columns under compression plus minor axis bending

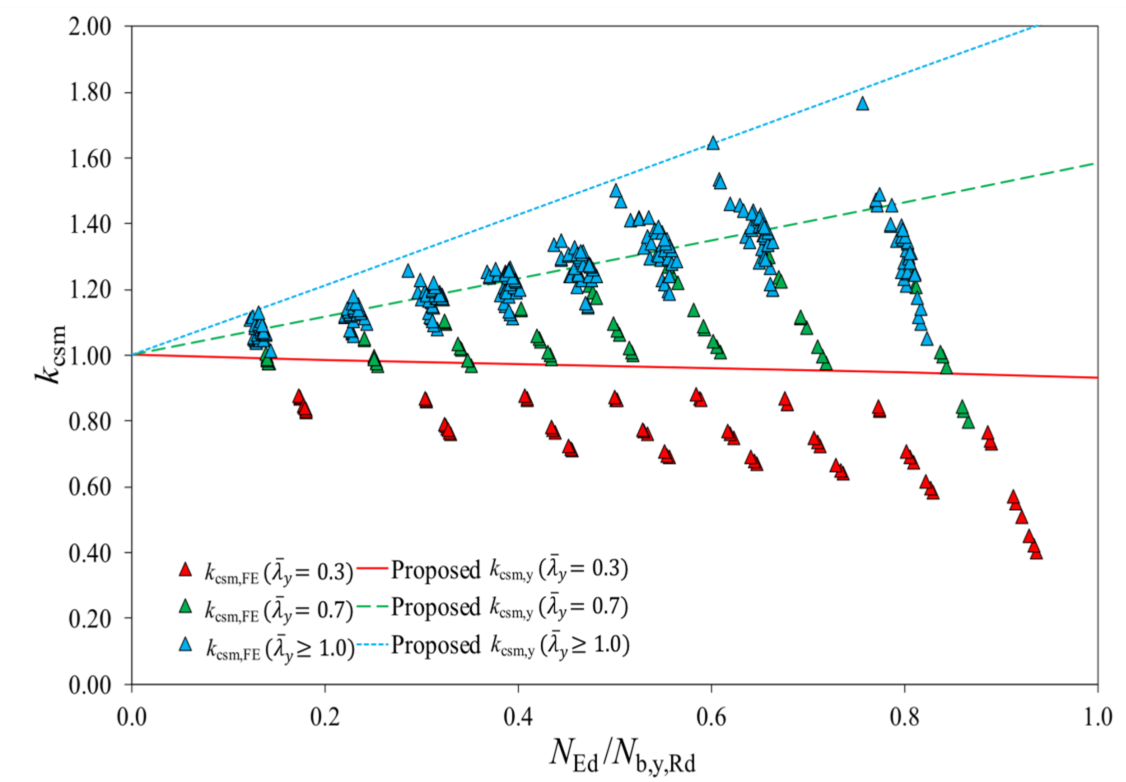

Fig. 17. Proposed CSM interaction factor for S960 welded-I section beam-columns under compression plus major axis bending

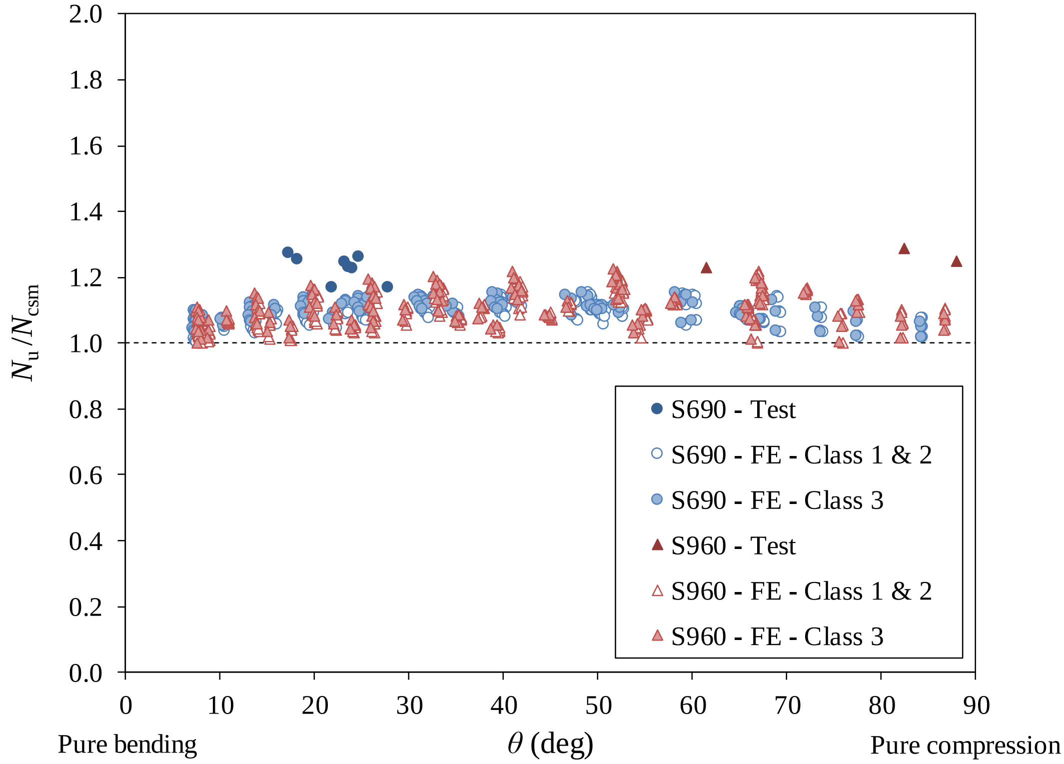

Fig. 18. Comparison of test and FE results with design resistances predicted by the proposed CSM based method for HSS welded I-sections under compression plus minor axis bending

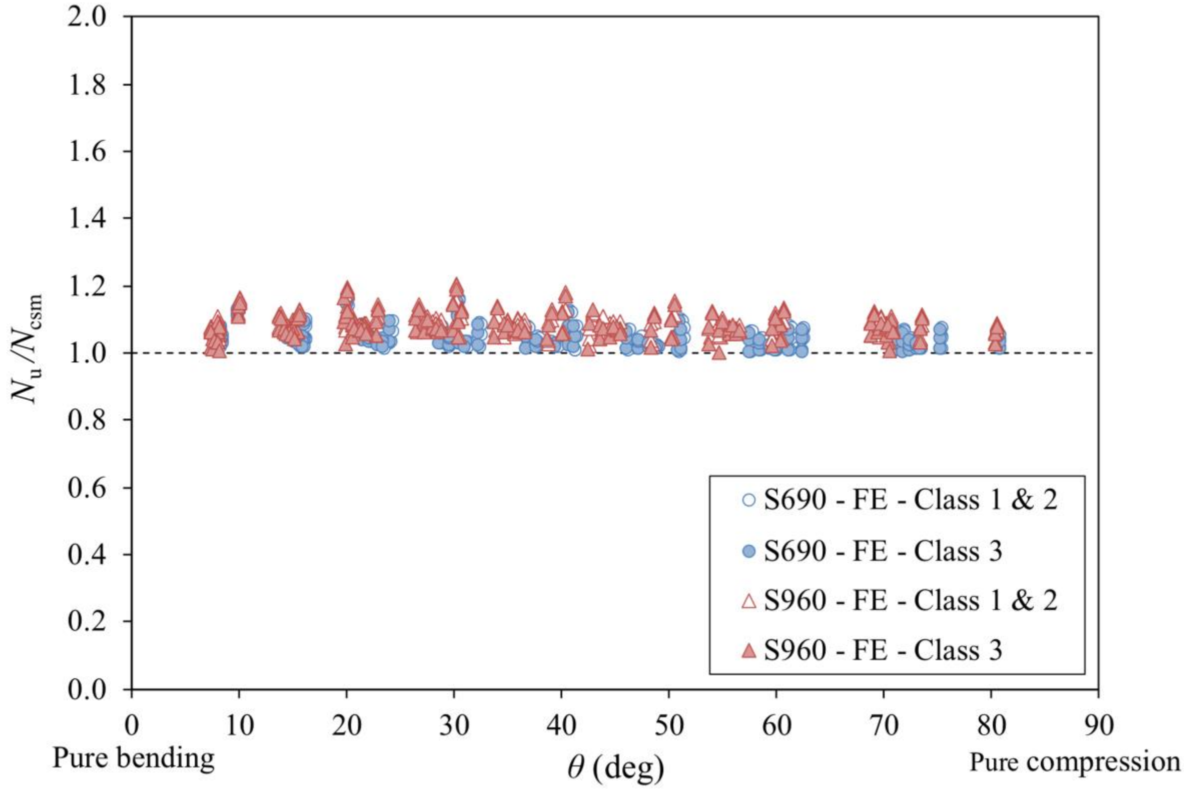

Fig. 19. Comparison of FE results with design resistances predicted by the proposed CSM based method for HSS welded I-sections under compression plus major axis bending

Tables:

Table 1: Summary of tensile coupon test results [27,32]

Steel grade	t (mm)	E (N/mm²)	f_y (N/mm²)	f_u (N/mm²)	ε_u
S690	6	210000	766	815	0.059
	10	212000	756	793	0.070
	16	209000	800	844	0.066
S960	14	208000	973	1052	0.019

Table 2: Measured geometric dimensions, global imperfection amplitudes and load eccentricities of test specimens [27,32]

Steel grade	Specimen	H (mm)	B (mm)	t_f (mm)	t_w (mm)	L (mm)	L_{eff} (mm)	$\|\delta\|/L_{eff}$ ($\times 10^{-4}$)	e (mm)
S690	EH1P	140.0	119.6	9.90	5.83	1612.0	1992.0	1.0	101.5
	EH1Q	141.2	119.8	9.91	5.85	2410.1	2790.1	2.0	96.1
	EH2P	170.0	149.3	9.90	5.81	1613.3	1993.3	1.0	103.8
	EH2Q	170.0	149.7	9.92	5.85	2410.3	2790.3	2.0	99.7
	EH3P	231.8	201.5	15.98	9.92	1613.3	1993.3	< 0.25	98.2
	EH3Q	231.7	200.7	15.97	9.95	2412.6	2791.6	4.0	102.4
	EH4P	284.2	250.1	15.97	9.92	1611.5	1990.5	3.0	100.1
	EH4Q	282.0	249.9	15.93	9.93	2410.1	2790.1	< 0.25	98.6
S960	H1-960	211.1	209.8	13.96	13.93	1542.5	1882.5	3.6	19.3
	H2-960	209.5	210.8	13.93	13.93	2543.7	2883.7	2.3	4.3
	H3-960	209.9	211.0	13.92	13.87	4041.5	4381.5	6.9	1.8

Table 3: Comparison of the experimental and numerical ultimate loads [27,32]

Steel grade	Specimen	$N_{u,test}$ (kN)	$N_{u,FE}$ (kN)	$N_{u,test}/N_{u,FE}$
S690	EH1P	328	307	1.07
	EH1Q	250	252	0.99
	EH2P	527	493	1.07
	EH2Q	418	413	1.01
	EH3P	1698	1655	1.03
	EH3Q	1376	1310	1.05
	EH4P	2660	2583	1.03
	EH4Q	2276	2169	1.05
			Mean	1.04
			COV	0.03
S960	H1-960	4683	4534	1.03
	H2-960	4282	3994	1.07
	H3-960	2323	2142	1.08
			Mean	1.06
			COV	0.03

Table 4: Geometric dimensions and key parameters employed in the parametric study

Steel grade	B (mm)	H (mm)	t_f (mm)	t_w (mm)	$\bar{\lambda}_{p,f}$	$\bar{\lambda}_{p,w}$	Cross-section class
			15.0	8.5	0.460	0.451	1
	150	150	14.2	8.3	0.486	0.468	2
			12.5	7.2	0.557	0.555	3
			15.0	14.0	0.442	0.445	1
S690	150	225	13.7	13.5	0.485	0.468	2
			12.5	11.9	0.538	0.537	3
			14.0	19.3	0.455	0.450	1
	150	300	13.2	18.6	0.485	0.470	2
			11.4	15.4	0.575	0.575	3
			17.6	9.4	0.436	0.438	1
	150	150	15.9	9.1	0.484	0.465	2
			13.8	7.8	0.563	0.562	3
			19.1	17.7	0.378	0.378	1
S960	150	225	15.2	14.9	0.486	0.468	2
			14.3	13.5	0.522	0.521	3
			16.8	23.2	0.412	0.411	1
	150	300	14.6	20.7	0.484	0.469	2
			13.5	18.3	0.533	0.534	3

Table 5: Comparison of test and FE results with predicted design resistances for HSS welded I-sections beam-columns under compression plus minor axis bending

Steel grade	N_u/N_{EC3}		N_u/N_{AISC}		N_u/N_{CSM}	
	Mean	COV	Mean	COV	Mean	COV
S690	1.150	0.145	0.988	0.101	1.095	0.030
S960	1.223	0.140	1.051	0.104	1.103	0.047

Table 6: Comparison of FE results with predicted design resistances for HSS welded I-sections beam-columns under compression plus major axis bending

Steel grade	N_u/N_{EC3}		N_u/N_{AISC}		N_u/N_{CSM}	
	Mean	COV	Mean	COV	Mean	COV
S690	1.087	0.057	1.081	0.065	1.041	0.030
S960	1.120	0.069	1.137	0.084	1.081	0.031

Table 7: Proposed coefficients for interaction curves (Eq. (17)) for different steel grades and loading cases

Steel grade	Loading cases	D_1	D_2	D_3
S690	Compression plus minor axis bending	2.88	0.48	1.15
	Compression plus major axis bending	1.15	0.40	0.99
S960	Compression plus minor axis bending	2.19	0.63	1.38
	Compression plus major axis bending	1.63	0.34	1.00

Table 8: Reliability analysis results for HSS welded I-section beam-columns under compression plus minor axis bending

Steel grade	Design method	No. of data	b	k_d	V_δ	γ_{M1}
S690	Eurocode 3	440	1.153	3.11	0.133	1.21
	AISC 360-16	440	0.988	3.11	0.095	1.26
	CSM	440	1.098	3.11	0.034	1.00
S960	Eurocode 3	435	1.224	3.11	0.130	1.21
	AISC 360-16	435	1.051	3.11	0.100	1.16
	CSM	435	1.105	3.11	0.048	1.07

Table 9: Reliability analyses results for HSS welded I-section beam-columns under compression plus major axis bending

Steel grade	Design method	No. of data	b	k_d	V_δ	γ_{M1}
S690	Eurocode 3	432	1.087	3.11	0.055	1.05
	AISC 360-16	432	1.081	3.11	0.063	1.07
	CSM	432	1.041	3.11	0.029	1.05
S960	Eurocode 3	432	1.120	3.11	0.065	1.10
	AISC 360-16	432	1.137	3.11	0.081	1.14
	CSM	432	1.081	3.11	0.031	1.06